Monthly Notices
of the
ROYAL ASTRONOMICAL SOCIETY

Mon. Not. R. Astron. Soc. **415,** 655–664 (2011) doi:10.1111/j.1365-2966.2011.18737.x

CO observations of high-z radio galaxies MRC 2104−242 and MRC 0943−242: spectral-line performance of the Compact Array Broadband Backend

B. H. C. Emonts,[1⋆†] R. P. Norris,[1] I. Feain,[1] G. Miley,[2] E. M. Sadler,[3] M. Villar-Martín,[4] M. Y. Mao,[1,5,6] T. A. Oosterloo,[7,8] R. D. Ekers,[1] J. B. Stevens,[1] M. H. Wieringa,[1] K. E. K. Coppin[9] and C. N. Tadhunter[10]

[1]*CSIRO Astronomy and Space Science, Australia Telescope National Facility, PO Box 76, Epping NSW 1710, Australia*
[2]*Leiden Observatory, University of Leiden, PO Box 9513, 2300 RA Leiden, Netherlands*
[3]*School of Physics, University of Sydney, NSW 2006, Australia*
[4]*Instituto de Astrofísica de Andalucía (CSIC), Aptdo. 3004, Granada, Spain*
[5]*School of Mathematics and Physics, University of Tasmania, Private Bag 37, Hobart 7001, Australia*
[6]*Australian Astronomical Observatory, PO Box 296, Epping, NSW 1710, Australia*
[7]*Netherlands Institute for Radio Astronomy, Postbus 2, 7990 AA Dwingeloo, the Netherlands*
[8]*Kapteyn Astronomical Institute, University of Groningen, PO Box 800, 9700 AV Groningen, the Netherlands*
[9]*Institute for Computational Cosmology, Durham University, South Road, Durham DH1 3LE*
[10]*Department of Physics and Astronomy, University of Sheffield, Sheffield S3 7RH*

Accepted 2011 March 17. Received 2011 March 17; in original form 2010 July 28

ABSTRACT

We present the first 7-mm observations of two high-redshift, Lyα-bright radio galaxies (MRC 2104−242 and MRC 0943−242) performed with the 2 × 2 GHz instantaneous bandwidth of the Compact Array Broadband Backend (CABB) at the Australia Telescope Compact Array (ATCA). The aim was to search for ^{12}CO(1−0) emission in these systems and test the millimetre capabilities of CABB for performing spectral line observations at high redshifts. We show that the stable band and enhanced velocity coverage of CABB, combined with hybrid array configurations, provide the ATCA with excellent 7-mm capabilities that allow reliable searches for the ground transition of CO at high redshifts. In this paper we explicitly discuss the calibration procedures used to reach our results. We set a firm upper limit to the mass of molecular gas in MRC 2104−242 ($z = 2.5$) of $M_{\rm H_2} < 2 \times 10^{10}\ (\alpha_x/0.8)\,{\rm M}_\odot$. For MRC 0943−242 ($z = 2.9$) we derive an upper limit of $M_{\rm H_2} < 6 \times 10^{10}\ (\alpha_x/0.8)\,{\rm M}_\odot$. We also find a tentative 3σ CO detection in the outer part of the giant Lyα halo that surrounds MRC 0943−242. The 30–33 GHz radio continuum of MRC 2104−242 and MRC 0943−242 is reliably detected. Both radio sources show a spectral index of $\alpha \approx -1.5$ between 1.4 and 30 GHz, with no evidence for spectral curvature within this range of frequencies.

Key words: techniques: interferometric – galaxies: active – galaxies: high-redshift – galaxies: individual: MRC 0943−242 – galaxies: individual: MRC 2104−242 – galaxies: ISM.

1 INTRODUCTION

Cold gas is a primary component in galaxy formation processes such as star formation and disc growth. However, despite detailed studies of cold gas in the nearby universe, it is still difficult to trace similar quantities of cold gas beyond our Galactic backyard. Recently, Tacconi et al. (2010) and Daddi et al. (2010) observed that star-forming galaxies at high redshifts are likely to contain a much larger fraction of their total mass in the form of molecular gas compared with nearby massive spiral galaxies. Recent simulations support this idea that the molecular gas content of galaxies increases when going to higher redshifts (Obreschkow & Rawlings 2009a,b; Obreschkow et al. 2009a,b). These results demonstrate that extensive studies of cold molecular gas in the early Universe are becoming feasible with existing radio telescopes.

Powerful radio galaxies enable comprehensive studies of the cold ISM throughout the Universe. Their strong radio sources provide a background continuum against which we can search for

⋆E-mail: bjorn.emonts@csiro.au
†Bolton Fellow.

foreground neutral and molecular gas in absorption (e.g. Uson, Bagri & Cornwell 1991; Vermeulen et al. 2003; Carilli et al. 2007; Kanekar, Chengalur & Lane 2007), while their host galaxies are generally in a very specific stage of galaxy evolution. Detailed studies at low and intermediate redshifts reveal that powerful radio galaxies are frequently associated with gas-rich galaxy mergers (e.g. Heckman et al. 1986; Baum, Heckman & van Breugel 1992), often contain young stellar populations (Tadhunter et al. 2005; Holt et al. 2007; Labiano et al. 2008), and many display strong jet–ISM interactions (Tadhunter 1991; Clark et al. 1998; Villar-Martín et al. 1999; Emonts et al. 2005; Morganti et al. 2005a; Morganti, Tadhunter & Oosterloo 2005b; Holt, Tadhunter & Morganti 2008). At high redshifts ($z > 2$), luminous radio galaxies ($L_{500\,\mathrm{MHz}} > 10^{27}\,\mathrm{W\,Hz^{-1}}$) are among the most massive galaxies in the early Universe (see Miley & De Breuck 2008, for a review). They are typically surrounded by protoclusters, which are thought to be the ancestors of rich local clusters (e.g. Pentericci et al. 2000a; Venemans et al. 2007). The high-z radio galaxies and surrounding protocluster gas and galaxies often interact with one another (e.g. Ivison et al. 2008; Nesvadba et al. 2008) and are therefore laboratories for studying the formation and evolution of galaxies and clusters as well as investigating the relationship between early star formation and active galactic nuclear (AGN) activity.

Since Brown & Vanden Bout (1991) first observed CO gas (the strongest tracer for molecular hydrogen) at a redshift beyond $z = 2$, intensive searches for CO in high-z radio galaxies during the early 1990s were unsuccessful (Evans et al. 1996; van Ojik et al. 1997). Since then, studies of individual radio galaxies at $z \sim 2$–5 with synthesis radio telescopes have found CO emission (tracing molecular gas masses of a few $\times\ 10^{10}$–$10^{11}\,\mathrm{M_\odot}$) in a number of these systems (e.g. Scoville et al. 1997; Papadopoulos et al. 2000; De Breuck et al. 2003a; De Breuck, Neri & Omont 2003b; De Breuck et al. 2005; Klamer et al. 2005; Nesvadba et al. 2009; see also Solomon & Vanden Bout 2005; Omont 2007; Miley & De Breuck 2008 for reviews). In some cases CO is observed to be resolved on scales of several tens of kpc (e.g. Papadopoulos et al. 2000). This indicates that large amounts of cold molecular gas may be relatively common in high-z radio galaxies. However, the major observational limitations for starting comprehensive studies of CO in high-z radio galaxies have been the very limited velocity coverage of existing millimetre-spectrometers (often not much wider than the velocity range of the CO gas and/or the accuracy of the redshift) plus the fact that most observatories can only target the higher order rotational transitions of ^{12}CO.

Although the higher order CO lines are likely to have a higher flux density than the lower ones in the nuclear starburst/AGN regions, where gas is dense and thermally excited, Papadopoulos et al. (2000, 2001) suggest that the opposite may be true for large reservoirs of less dense and subthermally excited gas that is more widely distributed. In fact, various studies of the low-order CO transitions in different types of high-z galaxies reveal molecular gas that is subthermally excited[1] (Greve, Ivison & Papadopoulos 2003; Hainline et al. 2006; Dannerbauer et al. 2009; Riechers et al. 2010) or distributed in extended reservoirs (Carilli et al. 2010; Daddi et al. 2010; Ivison et al. 2010, 2011). Cold CO gas distributed across the host galaxy may thus be much easier to detect in the lower CO transitions than generally assumed from studies of the higher transitions. Moreover, with uncertainties in excitation properties of the gas, observations of the rotational ground-transition of the CO molecule [^{12}CO(1−0) – referred to as CO in the remainder of this paper] provide the most accurate mass estimate of the overall molecular gas content in these systems.

Since 2009 April, the Australia Telescope Compact Array (ATCA) has a new broad-band backend system (the Compact Array Broadband Backend or CABB). CABB offers an instantaneous bandwidth of 4 GHz, split over 2 × 2 GHz observing bands, both with all Stokes polarization parameters and 2048 channels (i.e. spectral resolution of 1 MHz); see Ferris & Wilson (2002); Wilson et al. (2011). ATCA/CABB has millimetre observing capabilities at 3 mm (83.9–104.8 GHz), 7 mm (30.0–50.0 GHz) and 15 mm (16.0–25.0 GHz). This, in combination with hybrid array configurations with baselines as short as 31 m, makes the upgraded ATCA an excellent facility to detect and spatially resolve molecular gas in high-z radio galaxies by targeting the lower rotational CO transitions (see Section 2 for more details). A remarkable example of this is the recent detection of CO(2−1) in the distant ($z = 4.8$) submillimetre galaxy LESS J033229.4−275619 by Coppin et al. (2010).

To test the spectral-line performance of CABB over the 2 × 2 GHz bandwidth, we used the 7-mm band to search for CO(1−0) in two high-z radio galaxies from the Molonglo Reference Catalogue (McCarthy et al. 1990), namely MRC 2104−242 ($z = 2.5$) and MRC 0943−242 ($z = 2.9$). These two sources are a part of a larger sample of high-z radio galaxies that we aim to target with CABB in order to perform a systematic search for CO(1−0) in these systems.

MRC 2104−242 and MRC 0943−242 both have a redshift that corresponds to a critical epoch in galaxy formation ($z \sim 2.5$–3), at which there is a dramatic increase in submillimetre flux (Archibald et al. 2001; Smail et al. 2002; Chapman et al. 2005) and the space-density of (radio-loud) quasars reaches a maximum (e.g. Pei 1995; Shaver et al. 1996; Richards et al. 2006). *HST* observations by Pentericci et al. (2001) show that MRC 2104−242 and MRC 0943−242 both have an optical continuum that is clumpy and elongated in the direction of the radio source (Carilli et al. 1997; Pentericci et al. 2000b). Villar-Martín et al. (2003) show that they both contain a giant Lyα-halo ($\gtrsim$100 kpc in diameter). For MRC 2104−242 the Lyα gas is distributed roughly along the radio axis in what appears to be a rotating structure with a diameter $\gtrsim$120 kpc (Villar-Martín et al. 2006). MRC 0943−242 shows a quiescent Lyα-halo that extends well beyond the radio structure (Villar-Martín et al. 2003). MRC 0943−242 also shows a deep Lyα absorption (Rottgering et al. 1995; Jarvis et al. 2003), indicating that large amounts of neutral gas are present in this system. From fitting the spectral energy distributions of the host galaxies with *Spitzer*, Seymour et al. (2007) derive a total stellar mass of a few × $10^{11}\,\mathrm{M_\odot}$ for both the systems.

In Section 2 we present our CO observations and explain in more detail the enhanced capabilities of the ATCA for studying molecular gas at high redshifts. Section 3 shows the result regarding both the performance of CABB for doing these high-z CO studies and the scientific outcome of our observations of MRC 2104−242 and MRC 0943−242. In Sections 4 and 5 we discuss the scientific results and conclude that the upgraded ATCA is a world-class facility for spectral line observations of the cold molecular gas at high z.

2 OBSERVATIONS

During the period 2009 May–September , MRC 2104−242 and MRC 0943−242 were observed with ATCA/CABB. Details of the observations are given in Table 1.

[1] Harris et al. (2010) and Danielson et al. (2010) point out that a multicomponent interstellar medium, rather than subthermal excitation, may better reflect the physical properties of the molecular gas in high-z systems.

Table 1. Observations.

Source	Array	Obs. date	$t_{\rm int}$ (h)	$\nu_{\rm central}$ (GHz)
MRC 2104−242	H75	2009 July 21	6.99	33.000
		2009 July 23	4.15	33.020
	H168	2009 September 18	3.00	33.000
		2009 September 19	3.14	33.000
		2009 September 20	2.19	33.000
MRC 0943−242	H75	2009 July 11	3.10	30.001
		2009 July 12	3.20	30.010
		2009 July 14	2.88	30.001
	H168	2009 May 10	3.29	30.001
		2009 May 11	2.68	30.015
		2009 May 12	3.18	30.001

Notes. $t_{\rm int}$ is the effective on-source integration time (i.e. not including overheads).

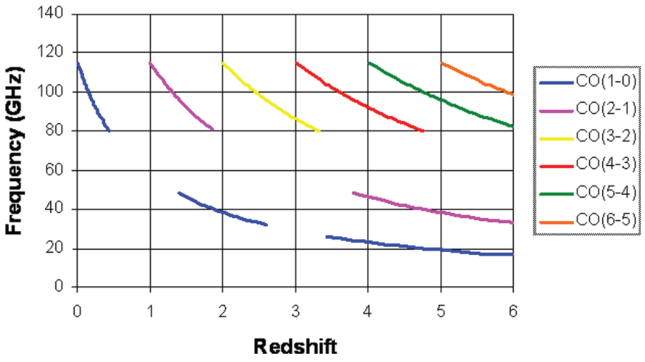

Figure 1. Observing frequency of the first six rotational transitions of CO that can be targeted with the CABB millimetre system (3, 7 and 15 mm) plotted against the redshift of the CO emitters.

Fig. 1 shows the observing windows for the various transitions of extragalactic CO currently available with CABB in the 3-, 7- and 15-mm bands. For MRC 2104−242 and MRC 0943−242 we targeted the ground-transition CO(1−0) with the CABB 7-mm system. The redshift of MRC 2104−242 ($z = 2.491$) corresponds to an observing frequency of 33.0 GHz, which is also one of the optimum CABB frequencies for centring the 7-mm band.[2] The redshift of MRC 0943−242 ($z = 2.9185$) corresponds[3] to an observing frequency of 29.4 GHz, which is outside the nominal 7-mm CABB band (30.0–50.0 GHz). Nevertheless, when centring the band at 30.001 GHz, data are obtained down to 29 GHz. Observations of MRC 0943−242 therefore served as a good test of how well the CABB system behaves at the very edge of the 7-mm band.

The total observing time for each source – including overhead and calibration – was roughly 40 h (see Table 1 and Section 2.1). The observations were spread over the two most compact hybrid array configurations (H75 and H168) in order to minimize the effect of atmospheric phase fluctuations (which worsen with the increase in baseline length; Klamer 2006). Both the array configurations include five antennas that are spread across both an east-west as well as a north–south spur. This ensures a reasonably good *uv* coverage (see Fig. 2) even from observing runs as short as 6–8 h, during which a source is targeted only above an elevation of 30° (in order to avoid high airmasses, which dramatically increase the system temperature; see Klamer 2006). The system temperatures ranged 70–132 K for the observations of MRC 2104−242 and 130–180 K for MRC 0943−242.[4]

At the high central frequencies of our observations (30–33 GHz), the coarsest spectral-line mode of CABB (2 × 2 GHz bands with 1 MHz spectral resolution) provides a velocity resolution of 9.5–11 km s^{-1} across an effective velocity coverage of at least 17 000 km s^{-1} per 2-GHz band. Both the 2-GHz bands were centred around the same observing frequency, but because they are not mutually independent, only one 2-GHz band was used in the final data analysis.

Observations were made as much as possible during the night and in good weather conditions (to avoid decorrelation due to atmospheric phase instabilities) and only above 30° elevation (to avoid high system temperatures due to large airmasses). Because our observations also served as a test for the performance of CABB for spectral-line observations, in the following section we will explain the details of several crucial calibration steps. For the data reduction and analysis we used MIRIAD and KARMA.

2.1 Calibration, overheads and data reduction

Our general observing strategy was as follows: a strong calibrator was observed at least three times during each run in order to check the reliability of the bandpass calibration. A secondary (phase/gain) calibrator was observed roughly every 10 min. Flux calibration was done at least once during each run. Pointing solutions of the antennas were checked and updated every hour, or every time the telescope slewed more than ∼20° on the sky. Taking into consideration the conservative nature of this calibration strategy, the overheads due to calibration and slewing were about 50 per cent.[5]

2.1.1 Phase/gain calibration

For phase calibration we performed a 2-min scan on a calibrator close to our target source roughly every 10 min, although target scans were decreased to 5 min in poor weather conditions and increased to 15 min when atmospheric phase stability was excellent. For MRC 2104−242 we used PKS B2008−159, PKS B2128−123 or PKS 2149−306 as phase calibrator. For MRC 0943−242 we used PKS 0919−260. Phase calibration was done in a standard way.

2.1.2 Bandpass calibration

In order to test the quality of the bandpass calibration at 7 mm across the full 2-GHz band, we observed a strong calibrator (PKS B0537−441, PKS B1253−055, PKS B1334−127, PKS B1921−293 or PKS B2223−052) at least three times during each run (unless the run was cut short due to weather). We noticed that weather and atmospheric conditions at the ATCA site can introduce frequency-dependent temporal gain fluctuations across the wide CABB band, which can have a significant effect on the quality of

[2] See the online ATCA Users Guide for details: http://www.narrabri.atnf.csiro.au/observing/users_guide/html/atug.html

[3] This redshift corresponds to the velocity of the most prominent H I absorption in the Lyα profile of MRC 0943−242 (Jarvis et al. 2003); see Section 2.1.3 for more details.

[4] More details on the theoretical estimates of $T_{\rm sys}$ values at 7 mm can be found in the online ATCA Users Guide.

[5] We estimate that in order to reach the potential maximum efficiency with less conservative calibration, overheads should be considered to be at least 30 per cent.

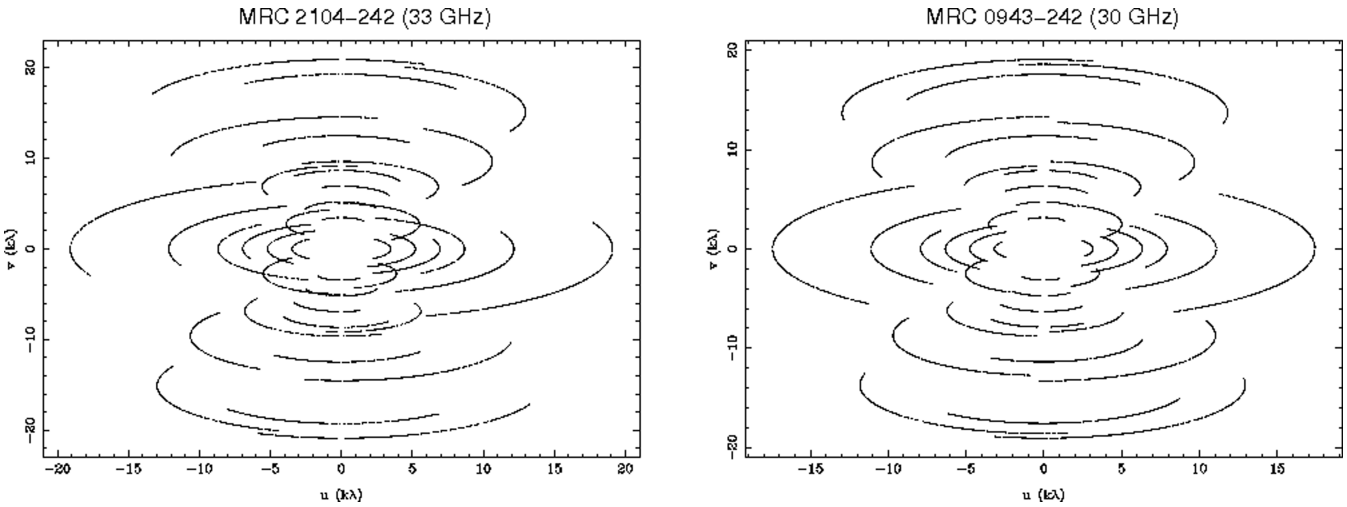

Figure 2. The *uv*-coverage of the combined observing runs of both MRC 2104−242 and MRC 0943−242 (Table 1), using the hybrid H75 and H168 arrays.

the bandpass calibration at 7 mm. It is therefore essential to obtain at least one good scan on the bandpass calibrator during good atmospheric conditions. For MRC 0943−242 we chose the best quality bandpass calibrator scan for calibrating our data. In case more than one bandpass calibrator scan was deemed suitable, we applied the bandpass solutions to that part of the data observed closest in time to the respective calibrator.

For MRC 2104−242 the strong phase calibrators PKS B2008−159 and PKS B2128−123 (with observed fluxes of $F_{33\,\mathrm{GHz}} \approx 1.9$ and 1.8 Jy, respectively) were suitable for bandpass calibration. This allowed us to obtain a bandpass solution roughly every 10-15 min. We used a new feature in the MIRIAD task MFCAL to interpolate between consecutive bandpass solutions in order to compensate for possible frequency-dependent gain variations that slowly fluctuate in time.

2.1.3 Flux calibration

For MRC 2104−242, flux calibration was done by observing Uranus at the time that it was at roughly the same elevation as the phase calibrator and target source during each run. The presence of a weak radio continuum from the lobe-dominated high-z radio galaxies in our 7-mm data (which are not expected to significantly change their flux densities over time-scales of a few months) allowed us to compare the relative flux calibration between the various runs, which remained constant within 15 per cent. Our absolute flux calibration used the available MIRIAD-model for Uranus. This model did not take into account changes in the planet's orientation, which introduce time variations of up to 10 per cent in its brightness temperature (see Kramer, Moreno & Greve 2008; Weiland et al. 2011), potentially leading to a significant error in absolute flux calibration. During one of the runs we also observed PKS B1934−638, which confirmed our Uranus-based absolute flux calibration to an accuracy of ∼18 per cent. We therefore estimate the overall (relative + absolute) uncertainty in the flux calibration of MRC 2104−242 to be within 30 per cent.

For MRC 0943−242, Uranus was not visible during our observing runs. For flux calibration we therefore observed the ultracompact H II region G309 [G309.9206+00.4790; Urquhart et al. (2007), with our pointing centred at RA(J2000) = 13:50:42.35, Dec(J2000) = −61:35:09.78] when it was at roughly the same elevation as the phase calibrator. We calibrated the flux of G309 against Uranus, which we observed roughly half a day later for each run. The flux of G309 was stable over our six observing epochs and the relative flux calibration between the six different runs was within 13 per cent. From our data we derive a value of $S_{30\,\mathrm{GHz}} = 1.31 \pm 0.07$ Jy for the shortest baselines at which the source is unresolved. Recently, Murphy et al. (2010) derived a flux density of $S_{32\,\mathrm{GHz}} = 1.1 \pm 0.11$ Jy for G309, also using Uranus as flux calibrator. In order to verify the accuracy of our absolute flux calibration, we observed PKS B1934−638 during three of our observing epochs. When using PKS B1934−638 as flux calibrator instead of Uranus, the absolute fluxes derived from our data are on average ∼15 per cent lower. This uncertainty in absolute flux calibration is consistent with the difference between our flux estimate for G309 (which we used to calibrate our data) and that made by Murphy et al. (2010). This may again reflects variations in the brightness of Uranus that were not accounted for by the existing models (see the preceding paragraph). The spectral index of G309 changes at most a few per cent across the 2-GHz band at 30 GHz, in agreement with Murphy et al. (2010). In all, we therefore estimate that for MRC 0943−242 the overall (relative + absolute) uncertainty in our flux calibration is within 30 per cent.

After flagging and bandpass, gain and flux calibration, we subtracted the continuum from the line data in the *uv* domain by applying a linear fit to the channels across the full 2-GHz band (for MRC 0943−242 we excluded from this fit the channels in which we found a tentative CO signal, see Section 3.3, although this has no significant effect when fitting the full 2-GHz band). Subsequently, a robust +1 weighted (Briggs 1995) continuum map and line data set were created by Fourier transforming the *uv* data and, in case of the continuum map, by cleaning the signal. We then translated the velocity axis to match the optical, barycentric rest-frame velocity at the redshift of MRC 2104−242 and MRC 0943−242. The redshift of MRC 2104−242 ($z = 2.491$) has been confirmed by Overzier et al. (2001) and Villar-Martín et al. (2003) through observations of the Lyα and various metal emission-lines. For MRC 0943−242, we chose to centre our observations on the redshift of the prominent H I absorption in the Lyα profile ($z = 2.9185$; Jarvis et al. 2003), which likely represents the bulk of the cold neutral gas in this system (see also De Breuck et al. 2003b). Table 2 shows details of the final data products that we obtained from our observations (some of these are described further in Section 3).

Table 2. Data.

	MRC 2104−242	MRC 0943−242
Effective int. time (h)	19.5	18.3
Target frequency (GHz)	33.02	29.417
Redshift	2.491	2.9185
Beam size (arcsec × arcsec)	11.7 × 7.6	11.5 × 9.0
Beam PA [PA (°)]	97.2	87.5
Δv (km s^{-1})	9.6	11.0
$\sigma_{\rm cont}$ (μJy bm^{-1})	29	33
$S_{\rm cont}$ (mJy)	4.0	3.3
$\sigma_{\rm line}$ (mJy bm^{-1} ch^{-1})	0.45	0.90
$L'_{\rm CO}$ (K km s^{-1} pc^2)	$<2.6 \times 10^{10}$	$<7.3 \times 10^{10}$

Note. Effective int. time is the total effective on-source integration time of all runs in both configurations combined. Target frequency (GHz) is the observing frequency of the expected CO(1−0) line at the redshift of our sources (see text for details). Δv (km s^{-1}) is the velocity resolution per 1-MHz channel. $\sigma_{\rm cont}$ is the rms noise level of the continuum image after $t_{\rm int}$. $S_{\rm cont}$ is the integrated continuum flux of the radio source at the target frequency. $\sigma_{\rm line}$ is the rms noise level of the full-resolution line data per 1-MHz channel after $t_{\rm int}$. $L'_{\rm CO}$ gives the upper limit on the CO luminosity (see text for details).

3 RESULTS

3.1 CABB performance

Fig. 3 shows the 33-GHz radio continuum map of MRC 2104−242 and a spectrum at the location of the centre of the host galaxy. The continuum image has an rms noise level of 29 μJy beam^{-1} (after $t_{\rm int} = 19.5$ h; see Table 2), demonstrating the effectiveness of ATCA/CABB for deep millimetre continuum studies. The 2-GHz spectrum has a large velocity coverage of ∼17 000 km s^{-1} with an rms noise in each 1-MHz channel ($\Delta v = 9.6$ km s^{-1}) of $\sigma = 0.45$ mJy bm^{-1}, with no significant systematic bandpass effects.

Fig. 4 shows the 30-GHz radio continuum map of MRC 0943−242 (with an rms noise of 33-μJy beam^{-1}) and an off-nuclear spectral line profile. In this case, at the edge of the 7-mm band, half the observing band lies outside the nominal CABB range (Section 2), where there are instrumental low-level structures in the noise or in the bandpass at about the 1σ level of the full (1 MHz) resolution data (Fig. 4b). In addition, the noise starts to vary beyond the nominal CABB range (Fig. 4c). After an effective on-source integration time of 18.3 h, we derive a noise level at 29.4 GHz of $\sigma = 0.9$ mJy bm^{-1} per 1-MHz channel ($\Delta v = 11$ km s^{-1}), i.e. twice the noise level at the optimum observing frequency of 33 GHz (see above). However, as can be seen in the Hanning-smoothed data of Fig. 4(c), the noise level peaks at our target frequency of 29.4 GHz and is significantly lower throughout most part of the band, even below the nominal edge of 30 GHz. We therefore conclude that up to ∼0.8 GHz below the nominal 7-mm band, CABB is still suitable for spectral-line work.

Coppin et al. (2010) detected CO(2−1) in a $z = 4.8$ submillimetre galaxy, which was observed with CABB at 40.0 GHz (i.e. towards the other end of the 7-mm band compared to our 33/30 GHz observations). They find noise levels of $\sigma \approx 0.44$ mJy bm^{-1} per 1-MHz channel and a bandpass stable enough to detect their CO signal at about the 5σ level when binning across >10 channels. The data quality at 40 GHz thus appears comparable to that at 33 GHz as presented in this paper, giving a good indication for the excellent performance of CABB across the entire ATCA 7-mm band.

3.2 MRC 2104−242

MRC 2104−242 (Fig. 3*a*) is resolved at 33 GHz with a total flux of 3.5 mJy. The continuum structure consists of two components on either side of the optical host galaxy, in agreement with 4.7 and 8.2 GHz VLA continuum observations that identified it as a double-lobed radio source (Pentericci et al. 2000b). The bright northern lobe has a peak flux density of $S_{33\,\rm GHz} = 2.7$ mJy bm^{-1}, while

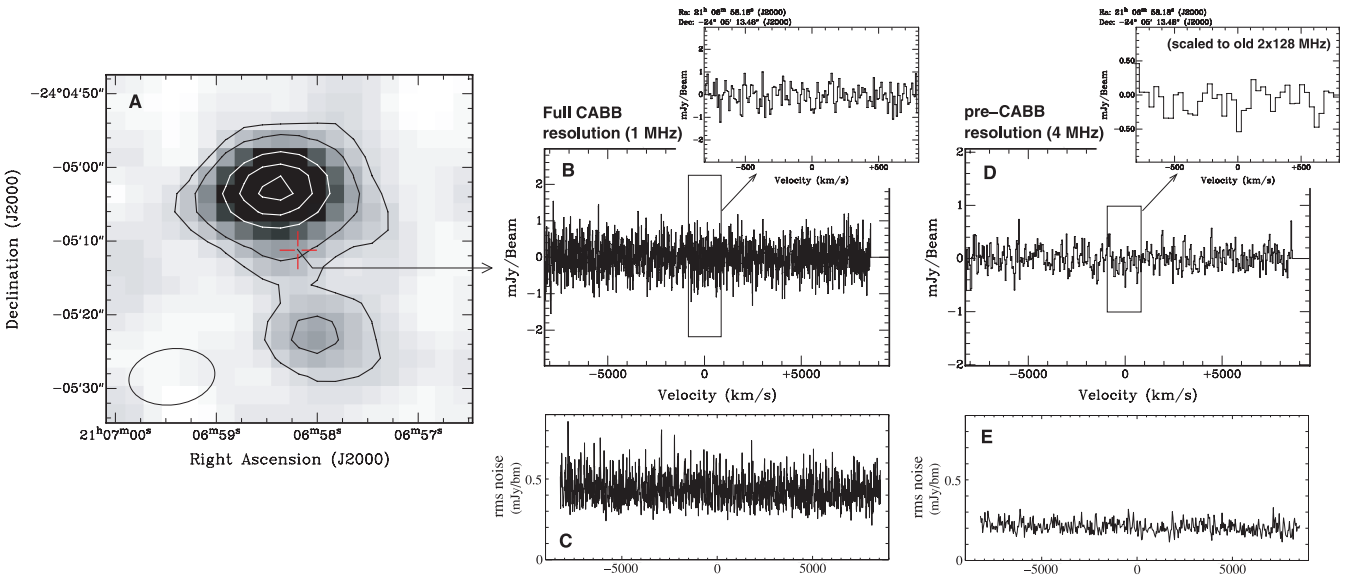

Figure 3. (a) 33-GHz radio continuum map of MRC 2104−242 (contour levels: 0.1, 0.3, 1.0, 1.7, 2.4 mJy bm^{-1}). The red cross indicates the location of the radio host galaxy. (b) spectral line profile against the centre of the radio host galaxy. Shown is the full 1-MHz velocity resolution of CABB across the 2-GHz band. The *x*-axis shows the velocity in the rest frame of the radio host galaxy (see Section 2.1.3). The zoom-in shows a portion of the CABB data with the approximate bandwidth coverage of the old pre-CABB ATCA system (2 × 128 MHz). (c) rms noise per 1-MHz channel in the region of the radio source. (d) Same as panel (b), but data binned to 4-MHz channels (i.e. similar to the pre-CABB system; the zoom-in therefore gives a good representation of the data that could be obtained with the old 2 × 128 MHz pre-CABB backend). (e) rms noise per channel of 4 MHz in the region of the radio source.

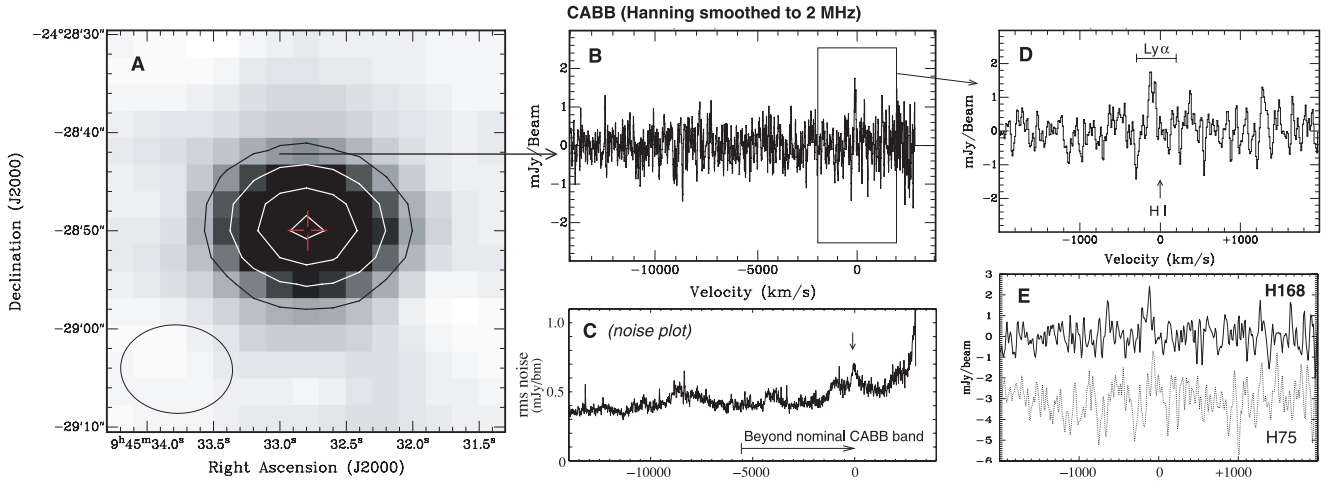

Figure 4. (a) 30-GHz radio continuum map of MRC 0943−242 (contour levels: 0.4, 1.0, 2.0, 3.0 mJy bm^{-1}). The red cross indicates the location of the radio host galaxy. (b) Off-nuclear spectral line profile of redshifted CO. The spectrum is taken at the location marked by the arrow in panel (a) and Hanning smoothed to a velocity resolution of 2 MHz across the 2 GHz CABB band. The *x*-axis shows the optical barycentric velocity in the rest frame of the radio host galaxy (see Section 2.1.3). (c) rms noise per channel in the Hanning smoothed data of panel (b) across the CABB band, derived across the central region. The arrow marks the rms noise level at the velocity of the tentative CO detection (right-hand plot). (d). Zoom-in of panel (b), showing the tentative off-nuclear CO detection. The arrow indicates the redshift of the deep Lyα absorption of H I gas (Jarvis et al. 2003) at which we centred our zero velocity. The range of velocities of the emission-line gas in the giant Lyα halo (Villar-Martín et al. 2003) is also indicated in the plot. (e) separate data sets of the H75 and H168 array observations, both showing the tentative CO signal (for illustration purposes, the *x*-axis of the H75-array data is scaled-down by 3 mJy bm^{-1} in this plot).

the fainter southern lobe has $S_{33\,\mathrm{GHz}} = 0.39$ mJy bm^{-1}. Even at 33 GHz the radio continuum structure is dominated by the radio lobes and no core component (at the location of the optical nucleus) is seen in our data. We set a conservative upper limit to the 33 GHz core flux density of $S_{\mathrm{core-33\,GHz}} < 0.4$ mJy bm^{-1}. Fig. 5 shows that the integrated flux of MRC 2104−242 has a steep spectral index between 1.4 and 33.0 GHz, with $\alpha = -1.56$ (where $F_\nu \propto \nu^\alpha$). There is no evidence for spectral curvature within this range of frequencies. This is in agreement with spectral index observations of high-z ultrasteep spectrum radio sources by Klamer et al. (2006).

No CO is detected in MRC 2104−242, either at the location of the host galaxy or at the position of the radio source. We derive a firm upper limit on the CO emission-line luminosity in MRC 2104−242 by assuming a potential 3σ signal smoothed across 500 km s^{-1}, using

$$S_{\mathrm{CO}}\Delta V = 3\sigma\ \Delta v\ \sqrt{\frac{500\ \mathrm{km\ s^{-1}}}{\Delta v}}\ \mathrm{Jy\,km\,s^{-1}}, \quad (1)$$

with σ the noise level per 1 MHz channel in one beam (in Jy) and Δv the width of one 1-MHz channel (in km s^{-1}). The CO luminosity (upper limit) can then be calculated following Solomon & Vanden Bout (2005, and references therein):

$$L'_{\mathrm{CO}} = 3.25\times10^7 \left(\frac{S_{\mathrm{CO}}\Delta V}{\mathrm{Jy\,km\,s^{-1}}}\right)\left(\frac{D_{\mathrm{L}}}{\mathrm{Mpc}}\right)^2\left(\frac{\nu_{\mathrm{rest}}}{\mathrm{GHz}}\right)^{-2}(1+z)^{-1}, \quad (2)$$

with L'_{CO} expressed in K km s^{-1} pc^2 and with $D_{\mathrm{L}} = 20\,018$ Mpc the luminosity distance of MRC 2104−242 (following Wright 2006).[6]

[6] See http://www.astro.ucla.edu/∼wright/CosmoCalc.html for Ned Wright's online cosmology calculator that we used to derive luminosity and angular-size distances. Throughout this paper we use $H_0 = 71$ km s^{-1} Mpc^{-1}, $\Omega_{\mathrm{M}} = 0.3$ and $\Omega_\Lambda = 0.7$.

For MRC 2104−242, $S_{\mathrm{CO}}\Delta V < 0.094$ Jy km s^{-1}, hence $L'_{\mathrm{CO}} < 2.6\times10^{10}$ K km s^{-1} pc^2.

3.3 MRC 0943−242

The radio source MRC 0943−242 (Fig. 4a) has a flux density of 3.3 mJy bm^{-1} and is unresolved in our data. Higher resolution continuum observations at 4.7 and 8.2 GHz by Carilli et al. (1997) show that the radio source consists of two lobes that are separated by 4 arcsec. When comparing the flux of our 30-GHz data with the integrated flux at 1.5, 4.7 and 8.2 GHz (Carilli et al. 1997), Fig. 5 shows that MRC 0943−242 has a steep spectral index between 1.5 and 30 GHz with $\alpha = -1.44$. Similar to the case of MRC 2104−242, there is no evidence for spectral curvature within this range of frequencies.

No CO is detected at the central (nuclear) location of MRC 0943−242. When estimating an upper limit on L'_{CO} in MRC 0943−242 (potential 3σ detection smoothed across 500 km s^{-1}), we derive $L'_{\mathrm{CO}} < 7.3\times10^{10}$ K km s^{-1} pc^2 (for $D_{\mathrm{L}} = 24242$ Mpc, which corresponds to an angular-size scale of 7.65 kpc arcsec^{-1} for MRC 0943−242; Wright 2006).

3.3.1 Tentative off-nuclear CO detection

As can be seen in Figs 4(b), (d) and (e), we find a tentative, off-nuclear 3σ CO(1−0) detection in the Hanning smoothed data of MRC 0943−242 (with σ the noise level at the frequency that corresponds to the tentative detection; see the arrow in Fig. 4c). The tentative CO signal spreads over an area about the size of one synthesized beam roughly 60 kpc north-east (NE) of the centre of the host galaxy. It peaks at $v \sim -100$ km s^{-1} with a flux density of ∼1.8 mJy bm^{-1}(with a tentative second peak present at the 1 mJy bm^{-1} level around $v \sim -500$ km s^{-1}). The estimated luminosity of the tentative double-peaked CO signal is

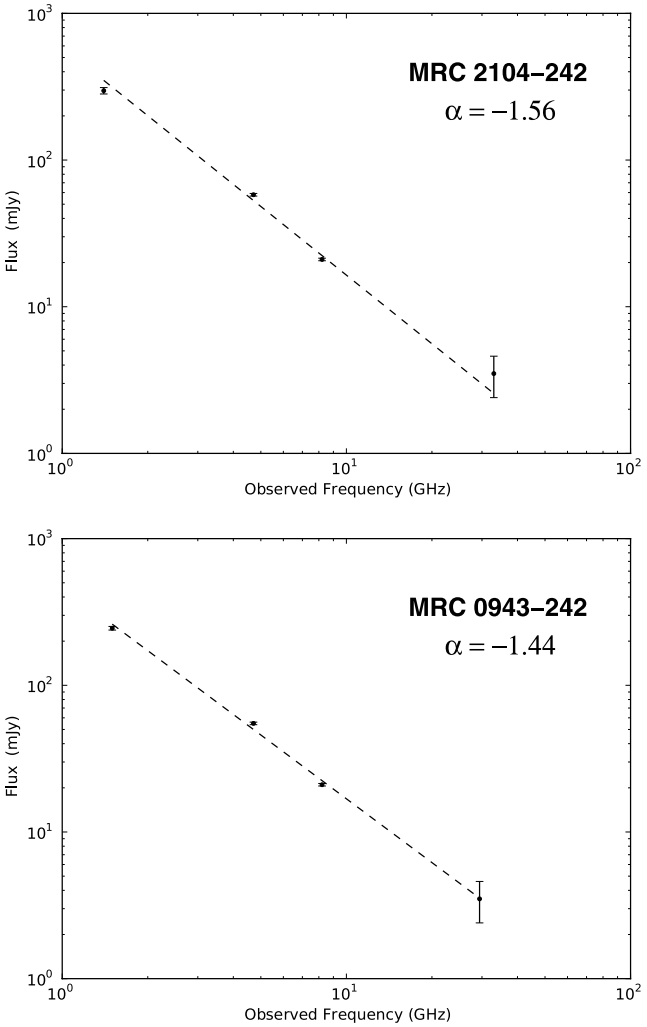

Figure 5. Spectral index of MRC 2104−242 (top) and MRC 0943−242 (bottom). Shown is the total integrated flux. Data at 1.4, 4.7 and 8.2 GHz are taken from Carilli et al. (1997) and Pentericci et al. (2000b), with errors corresponding to 2 per cent of the flux at these wavelengths (as estimated by Carilli et al. 1997).

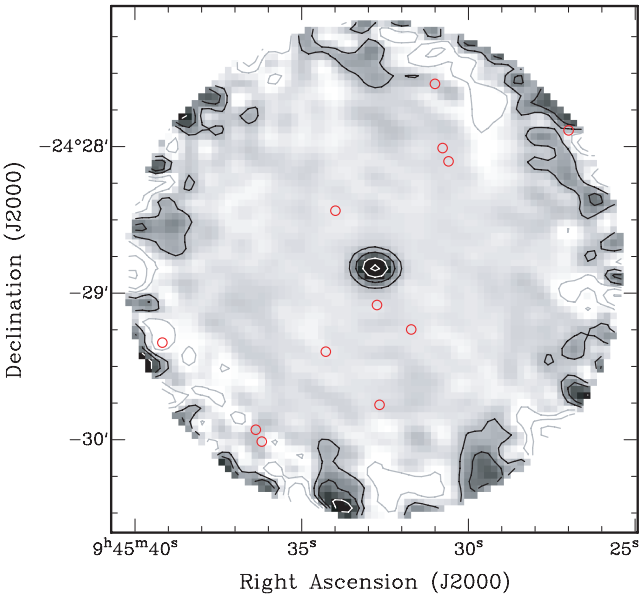

Figure 6. Continuum image of MRC 0943−242. Shown is an area the size of the FWHM of the ATCA's primary beam at 30 GHz. Flux densities are corrected for the primary beam response pattern, which causes the effective noise level to rise significantly towards the edge of the image. Contours: −0.4, −1.0, −2.0 (grey); 0.4, 1.0 2.0, 3.0 (black/white) mJy bm^{-1}. The red circles indicate the 12 Lyα-bright galaxies in the field of MRC 0943−242 (and with redshifts within the CABB observing band) detected by van Breukelen et al. (2005) and Venemans et al. (2007).

$L'_{\rm CO} \sim 8 \times 10^{10}$ K km s^{-1} pc^2 (equation 2). Both the H75 and H168 array data show indications for this tentative CO signal (Fig. 4*e*). However, because of the low-level (1σ) structure in the noise/bandpass beyond the nominal 7-mm observing band (see Section 3.1), our results did not improve by further smoothing/binning the data in velocity. Our tentative 3σ detection thus needs to be verified with additional observations before conclusions can be drawn.

3.4 The environments of high-*z* radio galaxies

The large instantaneous velocity coverage of CABB (see Section 2) also makes it possible to search for CO emitters in the field of our high-*z* radio galaxies. The full width at half-maximum (FWHM) of the primary beam is 87/95 arcsec at 33/30 GHz, corresponding to about 0.69/0.73 Mpc at the redshift of MRC 2104−242/MRC 0943−242.

High-*z* radio galaxies are generally located in protocluster environments (e.g. Pentericci et al. 2000a; Venemans et al. 2007). MRC 0943−242 is known to be located in a protocluster with many nearby companions detected in Lyα and with known redshifts (Venemans et al. 2007). There are 12 known Lyα companions within the primary beam and observing band of our observations (van Breukelen, Jarvis & Venemans 2005; Venemans et al. 2007, see also Fig. 6). None of these galaxies shows a clear CO detection above a 3σ limit, after correcting for primary beam attenuation.

Lyα observations of the environment of MRC 2104−242 are lacking and hence the cluster properties are unknown. No CO was detected within the primary beam above 3σ after correcting for primary beam attenuation.

4 DISCUSSION

4.1 H_2 masses

CO is an excellent tracer of molecular hydrogen, because the rotational transitions of CO are excited primarily by collisions with H_2. A standard conversion factor $\alpha_x = M_{\rm H_2}/L'_{\rm CO}$ [M$_\odot$ (K km s^{-1} pc^2)$^{-1}$] is generally used to calculate the mass of the cold molecular gas (where $M_{\rm H2}$ includes a fraction of the molecular gas that is in the form of helium – see for example Solomon & Vanden Bout 2005, for a review). For ultraluminous infrared galaxies (ULIRGs), Downes & Solomon (1998) derived a conversion factor of $\alpha_x \sim 0.8$ M$_\odot$ (K km s^{-1} pc^2)$^{-1}$. This is in agreement with other observations of ULIRGs (Solomon et al. 1997; Evans et al. 2002) as well as high-*z* submillimetre and star-forming galaxies (Stark et al. 2008; Tacconi et al. 2008), which imply that $\alpha_x \sim$ 0.8–1.6 M$_\odot$ (K km s^{-1} pc^2)$^{-1}$. We adopt a value of $\alpha_x = 0.8$ M$_\odot$ (K km s^{-1} pc^2)$^{-1}$ also for the two high-*z* radio galaxies that we study in this paper. We note, however, that there is a significant uncertainty in this conversion factor, since values as high as $\alpha_x \sim 5$ have

been derived for molecular clouds in the Milky Way (Scoville et al. 1987; Strong et al. 1988, see also Dickman 1978; Bloemen et al. 1986; Solomon et al. 1987) as well as other nearby spiral galaxies (Dickman, Snell & Schloerb 1986; Solomon & Barrett 1991).

Based on our 3σ upper limits on $L'_{\rm CO}$ and assuming $\alpha_x = 0.8$, we estimate that $M_{\rm H_2} < 2 \times 10^{10}\,{\rm M}_\odot$ for MRC 2104−242 and $M_{\rm H_2} < 6 \times 10^{10}\,{\rm M}_\odot$ for MRC 0943−242. The tentative off-nuclear CO detection in MRC 0943−242 has an estimated molecular gas mass of $M_{\rm H_2} = 6 \times 10^{10}\,{\rm M}_\odot$.

4.2 Molecular gas properties of high-z radio galaxies

The upper H_2 mass limits that we derive for MRC 2104−242 and MRC 0943−242 are comparable to H_2 masses derived from CO detections in high-z radio galaxies (e.g. Scoville et al. 1997; Papadopoulos et al. 2000; De Breuck et al. 2003a; De Breuck, Neri & Omont 2003b; De Breuck et al. 2005; Klamer et al. 2005; Nesvadba et al. 2009, see also Solomon & Vanden Bout 2005; Miley & De Breuck 2008 for reviews). However, as discussed in Section 1, most of these observations have targeted the higher rotational CO transitions, which could underestimate the total molecular gas content in these systems. CO(1−0) detections have been claimed for two high-z radio galaxies, namely 4C 60.07 ($z = 3.8$, Greve, Ivison & Papadopoulos 2004) and TNJ 0924−2201 ($z = 5.2$, Klamer et al. 2005), both with $M_{\rm H2} = 1 \times 10^{11}\,{\rm M}_\odot$. Our derived upper limit on molecular gas mass in MRC 2104−242 ($z = 2.491$) is a factor of 5 lower than this.

Submillimetre galaxies (SMGs) are likely merging systems with a short-lived burst of extreme star formation and are believed to be the progenitors of local massive ellipticals (e.g. Greve et al. 2005; Tacconi et al. 2008). In this sense, high-z radio galaxies and SMGs could be the same type of objects that differ only in their level of AGN activity (e.g. Reuland et al. 2007), although Ivison et al. (2008) argue that the violent AGN activity may occur predominantly during the early evolutionary stages of these systems. Greve et al. (2005) derived a median cold gas mass of $\langle M_{\rm H_2} \rangle = 3.0 \times 10^{10}\,{\rm M}_\odot$ among 12 SMGs detected in CO (see also Neri et al. 2003). This is of the same order as the upper limits that we derive for the mass of cold gas in MRC 2104−242 and MRC 0943−242.

Our derived upper limits on the molecular gas mass of MRC 2104−242 and MRC 0943−242 are *lower* than the H_2 mass estimates for a non-negligible fraction of normal massive star-forming galaxies at $z \sim 1$–2, derived from CO(3−2) observations by Tacconi et al. (2010, even when accounting for the much larger CO-to-H_2 conversion factor that they used). A similar result is seen by comparing the upper limits on CO in samples of high-z radio galaxies (Evans et al. 1996; van Ojik et al. 1997) with the results of Tacconi et al. (2010). Confirmation by observations of larger samples in the same CO transitions might indicate important differences in molecular gas fraction, excitation properties or chemical enrichment processes between high-z radio galaxies and distant massive star-forming galaxies.

The H_2 mass limit of MRC 2104−242 is only a factor of 3 higher than the H_2 content of the most CO-bright radio galaxies in the low-redshift Universe, as studied from CO(1−0) observatons of a large sample of IR-bright radio galaxies by Evans et al. (2005, corrected for the difference in the used α_x value and cosmological parameters). The vast majority of the low-z radio galaxies in the sample of Evans et al. (2005), however, contain significantly less molecular gas. This was recently confirmed by Ocaña Flaquer et al. (2010) with a large sample of low-z radio galaxies not selected on IR properties, for which they derive a median H_2 mass of only $M_{\rm H_2} = 2.2 \times 10^8\,{\rm M}_\odot$.

We note that many high-z CO detections to date are case studies of galaxies that were pre-selected based on their properties at other wavelengths, such as a large submillimetre dust content or a high infrared (IR) luminosity. Both at low and high z there appears to be a relation between the far-IR (FIR) and CO luminosity in different types of galaxies (see Evans et al. 2005; Greve et al. 2005, and references therein). Such a relation would indicate that (radio) galaxies with a FIR luminosity in the range of ULIRGs ($L_{\rm FIR} > 10^{12}\,{\rm L}_\odot$) contain a CO luminosity similar to the upper limit that we derive for MRC 2104−242 ($L'_{\rm CO} \sim$ few $\times\, 10^{10}\,{\rm K\,km\,s^{-1}\,pc^2}$). From *Spitzer* observations of MRC 0943−242 at 24, 70 and 160 μm (Seymour et al. 2007), we estimate an upper limit on the total IR luminosity of $L_{\rm TIR} < 2 \times 10^{13}\,{\rm L}_\odot$ when using the approximation by Dale & Helou (2002). Following the IR–CO relation found by Evans et al. (2005) and Greve et al. (2005), this IR limit corresponds to an average CO luminosity roughly a factor of 2 lower than the $L'_{\rm CO}$ upper limit that we derive for MRC 0943−242. The lack of detectable amounts of CO gas in MRC 0943−242 is therefore not unusual based on its IR properties, but it shows that unbiased CO(1−0) observations of high-z radio galaxies are becoming feasible.

Systematic searches for various CO transitions in unbiased samples of high-z (radio) galaxies are necessary to objectively investigate the overall content of cold molecular gas in the early Universe. Our results show that systematic and reliable searches for the ground-transition of CO in high-z (radio) galaxies are becoming feasible with existing broad-band facilities that can target the 20–50 GHz regime, such as the ATCA and EVLA.

4.2.1 *CO in the vicinity of MRC 0943−242?*

In this section we briefly discuss the possible nature of the tentative CO detection in the vicinity of MRC 0943−242, which needs to be confirmed before a more detailed analysis is deemed suitable.

The tentative CO detection (∼60 kpc NE of the host galaxy) may be associated with a nearby companion galaxy, although no companion has been detected in Lyα at that location (van Breukelen et al. 2005; Venemans et al. 2007), so any such galaxy would have to be Lyα-faint. Alternatively, the tentative CO detection may represent cold gas in the outer part of the quiescent Lyα halo (Villar-Martín et al. 2003). Binette et al. (2000) show that C IV absorption is associated with the deep Lyα absorption in MRC 0943−242 and derive that this reservoir of absorbing gas is also located in the outer halo (i.e. outside the radio cocoon). If confirmed, the cold gas properties of MRC 0943−242 would resemble those found in the high-z radio galaxies TXS 0828+193 ($z = 2.6$ Nesvadba et al. 2009) and B3 J2330+3927 ($z = 3.1$, De Breuck et al. 2003a).

The only two known high-z radio galaxies in which CO(1−0) has been detected (4C 60.07 and TNJ 0924−2201; see Section 4.2) also show indications that the CO gas may not be aligned with the central location of the host galaxy (Klamer et al. 2004; Ivison et al. 2008). In particular 4C 60.07 shows an apparent deficit of molecular gas in the radio host galaxy, while CO appears to be present in a merging companion and associated tidal debris (Ivison et al. 2008). If confirmed, a more detailed comparison between the CO(1−0) properties of these systems deserves further attention.

The position angle (PA) of the radio source in MRC 0943−242 (which has a total linear size of about 4 arcsec and is therefore unresolved in our observations) is PA = −74° (Carilli et al. 1997). This is roughly within 45° of the location of the tentative CO detection from the central region of the radio host galaxy. If confirmed,

this may resemble alignments that Klamer et al. (2004) argue exist among other high-z radio galaxies.

4.3 Radio continuum

Both radio sources are clearly detected in our sensitive ($\sigma \sim 30$ μJy) 7-mm continuum observations. Their spectral indices are relatively steep from ∼30 GHz down to 1.4 GHz, with no evidence for spectral curvature within this large range of frequencies. This indicates that there is no turnover due to synchrotron losses or inverse Compton cooling up to ∼115 GHz in the rest frame of these radio sources. This is consistent with continuum observations of a large sample of high-z ultrasteep spectrum radio galaxies by Klamer et al. (2006), who also find relatively steep power-law spectral energy distributions (SEDs) with no evidence for spectral steepening up to several tens of GHz in the rest frame. A detailed analysis of this phenomenon is crucial for understanding the electron acceleration mechanism or environmental properties of high-z radio sources, but is beyond the scope of this paper.

5 CONCLUSIONS

We presented the first 7-mm observations of two high-z radio galaxies (MRC 2104−242 and MRC 0943−242) with the 2 × 2 GHz Compact Array Broadband Backend. Our results demonstrate the feasibility of using ATCA/CABB for spectral-line work at high redshift. We also presented 7-mm continuum images of the two high-z radio galaxies, with a typical rms noise level of $\sim$30 μJy beam^{-1}. The enhanced spectral-line and continuum capabilities of ATCA/CABB in the millimetre regime complement those of other large existing and upcoming observatories, such as PdbI, EVLA and ALMA.

From our CO(1−0) data we derive upper limits on the H_2 mass of $M_{H_2} < 2 \times 10^{10}\,M_\odot$ for MRC 2104−242 and $M_{H_2} < 6 \times 10^{10}\,M_\odot$ for MRC 0943−242 ($\alpha_x = 0.8$). These upper limits are of the same order as H_2 mass estimates derived from CO detections of other high-z radio galaxies and SMGs, but lower than the mass of molecular gas detected in a non-negligible fraction of normal star-forming galaxies at $z \sim 1$–2. For MRC 0943−242 we also find a tentative CO(1−0) detection at about 60 kpc distance from the central region of the host galaxy, but this needs to be confirmed with additional observations.

The spectral index of both MRC 2104−242 and MRC 0943−242 is relatively steep with $\alpha \approx -1.5$ between 1.4 and 30 GHz. There is no evidence for spectral curvature up to ∼115 GHz in the rest frame of these radio sources.

ACKNOWLEDGMENTS

We are tremendously grateful to Warwick Wilson, Dick Ferris and their team and to the engineers and system scientists in Narrabri for making CABB such a great success. We also thank the anonymous referee for good suggestions that significantly improved this paper. The Australia Telescope is funded by the Commonwealth of Australia for operation as a National Facility managed by CSIRO.

REFERENCES

Archibald E. N., Dunlop J. S., Hughes D. H., Rawlings S., Eales S. A., Ivison R. J., 2001, MNRAS, 323, 417
Baum S. A., Heckman T. M., van Breugel W., 1992, ApJ, 389, 208
Binette L., Kurk J. D., Villar-Martín M., Röttgering H. J. A., 2000, A&A, 356, 23
Bloemen J. B. G. M. et al., 1986, A&A, 154, 25
Briggs D. S., 1995, PhD thesis, New Mexico Inst. Mining Technol.
Brown R. L., Vanden Bout P. A., 1991, AJ, 102, 1956
Carilli C. L., Roettgering H. J. A., van Ojik R., Miley G. K., van Breugel W. J. M., 1997, ApJS, 109, 1
Carilli C. L., Wang R., van Hoven M. B., Dwarakanath K., Chengalur J. N., Wyithe S., 2007, AJ, 133, 2841
Carilli C. L. et al., 2010, ApJ, 714, 1407
Chapman S. C., Blain A. W., Smail I., Ivison R. J., 2005, ApJ, 622, 772
Clark N. E., Axon D. J., Tadhunter C. N., Robinson A., O'Brien P., 1998, ApJ, 494, 546
Coppin K. et al., 2010, MNRAS, 407, L103
Daddi E. et al., 2010, ApJ, 713, 686
Dale D. A., Helou G., 2002, ApJ, 576, 159
Danielson A. L. R. et al., 2010, MNRAS, 1565
Dannerbauer H., Daddi E., Riechers D. A., Walter F., Carilli C. L., Dickinson M., Elbaz D., Morrison G. E., 2009, ApJ, 698, L178
De Breuck C. et al., 2003a, A&A, 401, 911
De Breuck C., Neri R., Omont A., 2003b, New Astron. Rev., 47, 285
De Breuck C., Downes D., Neri R., van Breugel W., Reuland M., Omont A., Ivison R., 2005, A&A, 430, L1
Dickman R. L., 1978, ApJS, 37, 407
Dickman R. L., Snell R. L., Schloerb F. P., 1986, ApJ, 309, 326
Downes D., Solomon P. M., 1998, ApJ, 507, 615
Emonts B. H. C., Morganti R., Tadhunter C. N., Oosterloo T. A., Holt J., van der Hulst J. M., 2005, MNRAS, 362, 931
Evans A. S., Sanders D. B., Mazzarella J. M., Solomon P. M., Downes D., Kramer C., Radford S. J. E., 1996, ApJ, 457, 658
Evans A. S., Mazzarella J. M., Surace J. A., Sanders D. B., 2002, ApJ, 580, 749
Evans A. S., Mazzarella J. M., Surace J. A., Frayer D. T., Iwasawa K., Sanders D. B., 2005, ApJS, 159, 197
Ferris R. H., Wilson W. E., 2002, URSI XXVIIth General Assembly, Poster 1629
Greve T. R., Ivison R. J., Papadopoulos P. P., 2003, ApJ, 599, 839
Greve T. R., Ivison R. J., Papadopoulos P. P., 2004, A&A, 419, 99
Greve T. R. et al., 2005, MNRAS, 359, 1165
Hainline L. J., Blain A. W., Greve T. R., Chapman S. C., Smail I., Ivison R. J., 2006, ApJ, 650, 614
Harris A. I., Baker A. J., Zonak S. G., Sharon C. E., Genzel R., Rauch K., Watts G., Creager R., 2010, ApJ, 723, 1139
Heckman T. M., Smith E. P., Baum S. A., van Breugel W. J. M., Miley G. K., Illingworth G. D., Bothun G. D., Balick B., 1986, ApJ, 311, 526
Holt J., Tadhunter C. N., González Delgado R. M., Inskip K. J., Rodriguez Zaurin J., Emonts B. H. C., Morganti R., Wills K. A., 2007, MNRAS, 381, 611
Holt J., Tadhunter C. N., Morganti R., 2008, MNRAS, 387, 639
Ivison R. J. et al., 2008, MNRAS, 390, 1117
Ivison R. J., Smail I., Papadopoulos P. P., Wold I., Richard J., Swinbank A. M., Kneib J., Owen F. N., 2010, MNRAS, 404, 198
Ivison R. J., Papadopoulos P. P., Smail I., Greve T. R., Thomson A. P., Xilouris E. M., Chapman S. C., 2011, MNRAS, 412, 1913
Jarvis M. J., Wilman R. J., Röttgering H. J. A., Binette L., 2003, MNRAS, 338, 263
Kanekar N., Chengalur J. N., Lane W. M., 2007, MNRAS, 375, 1528
Klamer I. J., 2006, PhD thesis, Univ. Sydney
Klamer I. J., Ekers R. D., Sadler E. M., Hunstead R. W., 2004, ApJ, 612, L97
Klamer I. J., Ekers R. D., Sadler E. M., Weiss A., Hunstead R. W., De Breuck C., 2005, ApJ, 621, L1
Klamer I. J., Ekers R. D., Bryant J. J., Hunstead R. W., Sadler E. M., De Breuck C., 2006, MNRAS, 371, 852
Kramer C., Moreno R., Greve A., 2008, A&A, 482, 359
Labiano A., O'Dea C. P., Barthel P. D., de Vries W. H., Baum S. A., 2008, A&A, 477, 491

McCarthy P. J., Kapahi V. K., van Breugel W., Subrahmanya C. R., 1990, AJ, 100, 1014
Miley G., De Breuck C., 2008, A&AR, 15, 67
Morganti R., Oosterloo T. A., Tadhunter C. N., van Moorsel G., Emonts B., 2005a, A&A, 439, 521
Morganti R., Tadhunter C. N., Oosterloo T. A., 2005b, A&A, 444, L9
Murphy T., Cohen M., Ekers R. D., Green A. J., Wark R. M., Moss V., 2010, MNRAS, 405, 1560
Neri R. et al., 2003, ApJ, 597, L113
Nesvadba N. P. H., Lehnert M. D., De Breuck C., Gilbert A. M., van Breugel W., 2008, A&A, 491, 407
Nesvadba N. P. H. et al., 2009, MNRAS, 395, L16
Obreschkow D., Rawlings S., 2009a, MNRAS, 400, 665
Obreschkow D., Rawlings S., 2009b, ApJ, 696, L129
Obreschkow D., Heywood I., Klöckner H., Rawlings S., 2009a, ApJ, 702, 1321
Obreschkow D., Klöckner H., Heywood I., Levrier F., Rawlings S., 2009b, ApJ, 703, 1890
Ocaña Flaquer B., Leon S., Combes F., Lim J., 2010, A&A, 518, A9
Omont A., 2007, Rep. Progress Phys., 70, 1099
Overzier R. A., Röttgering H. J. A., Kurk J. D., De Breuck C., 2001, A&A, 367, L5
Papadopoulos P. P., Röttgering H. J. A., van der Werf P. P., Guilloteau S., Omont A., van Breugel W. J. M., Tilanus R. P. J., 2000, ApJ, 528, 626
Papadopoulos P., Ivison R., Carilli C., Lewis G., 2001, Nat, 409, 58
Pei Y. C., 1995, ApJ, 438, 623
Pentericci L. et al., 2000a, A&A, 361, L25
Pentericci L., Van Reeven W., Carilli C. L., Röttgering H. J. A., Miley G. K., 2000b, A&AS, 145, 121
Pentericci L., McCarthy P. J., Röttgering H. J. A., Miley G. K., van Breugel W. J. M., Fosbury R., 2001, ApJS, 135, 63
Reuland M. et al., 2007, AJ, 133, 2607
Richards G. T. et al., 2006, AJ, 131, 2766
Riechers D. A., Carilli C. L., Walter F., Momjian E., 2010, ApJ, 724, L153
Rottgering H. J. A., Hunstead R. W., Miley G. K., van Ojik R., Wieringa M. H., 1995, MNRAS, 277, 389
Scoville N. Z., Yun M. S., Sanders D. B., Clemens D. P., Waller W. H., 1987, ApJS, 63, 821
Scoville N. Z., Yun M. S., Windhorst R. A., Keel W. C., Armus L., 1997, ApJ, 485, L21+
Seymour N. et al., 2007, ApJS, 171, 353
Shaver P. A., Wall J. V., Kellermann K. I., Jackson C. A., Hawkins M. R. S., 1996, Nat, 384, 439
Smail I., Ivison R. J., Blain A. W., Kneib J., 2002, MNRAS, 331, 495
Solomon P. M., Barrett J. W., 1991, in Combes F., Casoli F., eds, Proc. IAU Symp. 146, Dynamics of Galaxies and Their Molecular Cloud Distributions. Kluwer, Dordrecht, p. 235
Solomon P. M., Vanden Bout P. A., 2005, ARA&A, 43, 677
Solomon P. M., Rivolo A. R., Barrett J., Yahil A., 1987, ApJ, 319, 730
Solomon P. M., Downes D., Radford S. J. E., Barrett J. W., 1997, ApJ, 478, 144
Stark D. P., Swinbank A. M., Ellis R. S., Dye S., Smail I. R., Richard J., 2008, Nat, 455, 775
Strong A. W. et al., 1988, A&A, 207, 1
Tacconi L. J. et al., 2008, ApJ, 680, 246
Tacconi L. J. et al., 2010, Nat, 463, 781
Tadhunter C. N., 1991, MNRAS, 251, 46P
Tadhunter C., Robinson T. G., González Delgado R. M., Wills K., Morganti R., 2005, MNRAS, 356, 480
Urquhart J. S., Busfield A. L., Hoare M. G., Lumsden S. L., Clarke A. J., Moore T. J. T., Mottram J. C., Oudmaijer R. D., 2007, A&A, 461, 11
Uson J. M., Bagri D. S., Cornwell T. J., 1991, Phys. Rev. Lett., 67, 3328
van Breukelen C., Jarvis M. J., Venemans B. P., 2005, MNRAS, 359, 895
van Ojik R. et al., 1997, A&A, 321, 389
Venemans B. P. et al., 2007, A&A, 461, 823
Vermeulen R. C. et al., 2003, A&A, 404, 861
Villar-Martín M., Tadhunter C., Morganti R., Axon D., Koekemoer A., 1999, MNRAS, 307, 24
Villar-Martín M., Vernet J., di Serego Alighieri S., Fosbury R., Humphrey A., Pentericci L., 2003, MNRAS, 346, 273
Villar-Martín M. et al., 2006, MNRAS, 366, L1
Weiland J. L. et al., 2011, ApJS, 192, 19
Wilson W. E. et al., 2011, MNRAS, doi:10.1111/j.1365-2966.2011.18741.x
Wright E. L., 2006, PASP, 118, 1711

This paper has been typeset from a TEX/LATEX file prepared by the author.